A halogen budget of the bulk silicate Earth points to a history of early halogen degassing followed by net regassing

Meng Guo[a,1] and Jun Korenaga[a]

[a]Department of Earth and Planetary Sciences, Yale University, New Haven, CT 06520

Edited by T. Harrison, Department of Earth, Planetary, and Space Sciences, University of California, Los Angeles, CA; received September 1, 2021; accepted November 9, 2021

Halogens are important tracers of various planetary formation and evolution processes, and an accurate understanding of their abundances in the Earth's silicate reservoirs can help us reconstruct the history of interactions among mantle, atmosphere, and oceans. The previous studies of halogen abundances in the bulk silicate Earth (BSE) are based on the assumption of constant ratios of element abundances, which is shown to result in a gross underestimation of the BSE halogen budget. Here we present a more robust approach using a log-log linear model. Using this method, we provide an internally consistent estimate of halogen abundances in the depleted mid-ocean ridge basalts (MORB)-source mantle, the enriched ocean island basalts (OIB)-source mantle, the depleted mantle, and BSE. Unlike previous studies, our results suggest that halogens in BSE are not more depleted compared to elements with similar volatility, thereby indicating sufficient halogen retention during planetary accretion. According to halogen abundances in the depleted mantle and BSE, we estimate that ∼87% of all stable halogens reside in the present-day mantle. Given our understanding of the history of mantle degassing and the evolution of crustal recycling, the revised halogen budget suggests that deep halogen cycle is characterized by efficient degassing in the early Earth and subsequent net regassing in the rest of Earth history. Such an evolution of deep halogen cycle presents a major step toward a more comprehensive understanding of ancient ocean alkalinity, which affects carbon partitioning within the hydrosphere, the stability of crustal and authigenic minerals, and the development of early life.

mantle composition | halogen cycle | early Earth

The stable halogen elements (F, Cl, Br, and I) play a key role in a number of geochemical and biogeochemical systems. They affect the composition of hydrothermal fluids (e.g., ref. 1), the formation and transportation of ore minerals (e.g., refs. 2 and 3), the composition of magmas (e.g., ref. 4), and the pathways of biochemical reaction (e.g., refs. 5 and 6). Owing to their high volatility and incompatibility, halogens are also important tracers of planetary accretionary processes (e.g., ref. 7). A good understanding of halogen abundances in the bulk silicate Earth (BSE) and their current distribution among terrestrial reservoirs can help us track the history of interactions among mantle, crust, and hydrosphere (e.g., refs. 8–10).

Previous studies of halogen abundances in BSE (e.g., refs. 9 and 11–13) suggest that heavy halogens (Cl, Br, and I) display a noteworthy depletion compared to CI chondrites (14), by a factor of 30 to 50, which is far greater than expected from their condensation temperatures. Many attempts have been made to explain this severe depletion, including the models that require specific halogen behaviors during planetary accretionary processes (e.g., refs. 13 and 15–17) and the reevaluation of halogen abundances in chondritic meteorites (7). Also, with the current BSE composition models, ∼80 to 90% of Earth's halogens are concentrated in surface reservoirs (crust, oceans, and sediments) at present (e.g., refs. 9 and 18). This unusually high degassing fraction is suggested to conflict with the mantle degassing fraction of ∼50% based on argon-40 (19). Given that halogens are much more chemically active than argon, they can easily be incorporated into sediments, altered oceanic crust, and serpentinized mantle lithosphere and further be subducted into the mantle. Thus, their considerably high degassing fraction suggests unusual halogen behavior during Earth history (e.g., ref. 7). However, all of these efforts are built on the current estimates of BSE halogen budget. Therefore, there is an obvious impetus to examine the robustness of such estimates.

A common approach to estimate the halogen abundance in BSE employs the so-called constant ratio method (e.g., refs. 9, 11, and 12). This method assumes that the ratios of halogen and some reference elements in mid-ocean ridge basalts (MORB) and ocean island basalts (OIB) equal those in their respective source mantle. Thus, knowing the reference element concentration in the source mantle, the halogen concentrations can be calculated accordingly. This method relies on the reference elements that are expected to behave similarly to halogens during melting and crystallization (e.g., K, Rb, and Pr). Strictly speaking, however, the constant ratio method can adequately be applied only in one specific situation: when the bulk distribution coefficients of halogens and reference elements are the same during both mantle melting and magma crystallization. Only in this case, halogen and the reference element are linearly related, or in other words, the logarithmic slope of their covariation becomes unity. Unfortunately, such delicate equivalence is not observed in the MORB nor the OIB dataset (*SI Appendix*, Tables S1 and S2).

Significance

Halogens play a critical role in biochemistry and are useful to understand how planets formed and evolved. As we found that the traditional way of constraining the halogen budget within Earth is unreliable, we developed a method that better utilizes relevant geochemical data and estimated halogen abundances in various silicate reservoirs of Earth. Our halogen budget indicates that the majority of halogens are more concentrated in the mantle than in the surface and suggests that halogens have likely experienced early degassing and subsequent net regassing. This study also provides an important key to deciphering the geological history of ocean chemistry.

Author contributions: J.K. designed research; M.G. performed research; M.G. and J.K. analyzed data; M.G. wrote the paper; and J.K. discussed the results and commented on the manuscript.

The authors declare no competing interest.

This article is a PNAS Direct Submission.

[1]To whom correspondence may be addressed. Email: meng.guo@yale.edu.

This article contains supporting information online at http://www.pnas.org/lookup/suppl/doi:10.1073/pnas.2116083118/-/DCSupplemental.

Published December 16, 2021.

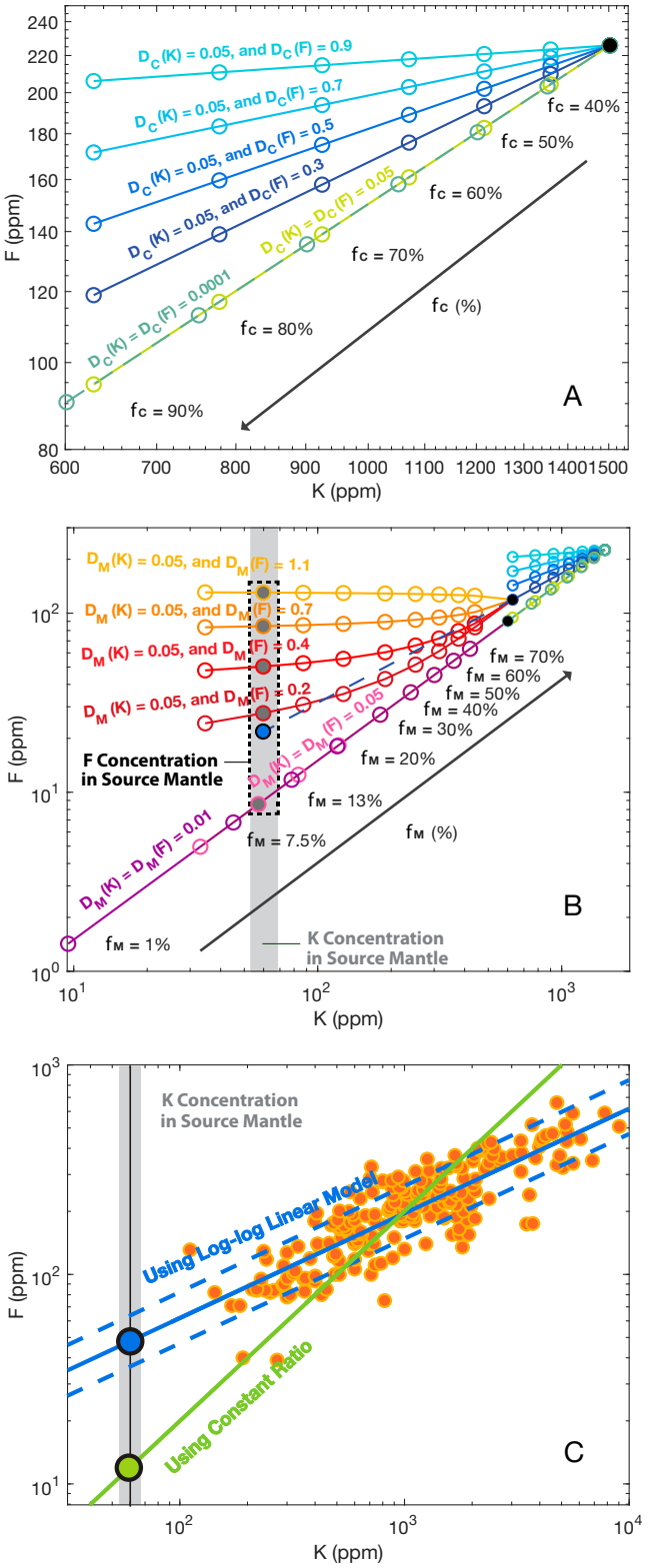

Fig. 1. Covariations of F versus K during mantle melting and fractional crystallization. (*A*) Logarithmic concentrations of F versus K in the primary melt of MORB. Different line colors correspond to different element bulk distribution coefficients during fractional crystallization. f_C is melt fraction during fractional crystallization. Black dot represents a sample composition of MORB. (*B*) Logarithmic concentrations of F versus K in the source mantle of MORB. Different line colors correspond to different element bulk distribution coefficients during mantle melting. f_M is melt fraction. Black dots are sample primary melt compositions taken from (*A*). Gray bar and dotted rectangle are K concentration range (25) and the calculated F concentration range in the source mantle of MORB, respectively. Blue dashed line and dot represent the results of the log-log linear model. (*C*) Comparison between the constant ratio method and the method based on a log-log linear model, which are shown in green and blue, respectively. Orange dots are the MORB data of F and K concentrations from PetDB (21). Gray bar is the K concentration range in the source mantle of MORB (25).

The limitation of the constant ratio method can be illustrated by modeling how halogen concentrations in MORB or OIB may be related to those in the respective source mantle through magma crystallization (Fig. 1*A*) and mantle melting (Fig. 1*B*). The calculated abundances of halogens and reference elements in the source mantle depend on their bulk distribution coefficients, and different assumptions on these distribution coefficients result in different slopes of covariations in the log-log space (Fig. 1 *A* and *B*). As noted before, the logarithmic slope of halogen and reference element is unity only when their bulk distribution coefficients are the same, and the slope deviates more from unity with increasingly dissimilar bulk distribution coefficients. As can be seen from the MORB and OIB datasets (*SI Appendix*, Tables S1 and S2), most of pairs of halogens and reference elements used in previous studies (e.g., F versus Pr, F versus K, Cl versus K, and Cl versus Rb) display nonlinear covariations, with their logarithmic slopes smaller than unity, which indicate considerably higher halogen concentrations in the source mantle compared with what the constant ratio method provides. In other words, the constant ratio method underestimates halogen abundances in the primary melt (Fig. 1*A*) and the source mantle (Fig. 1*B*) of MORB and OIB.

In light of this limitation of the constant ratio method, we have developed a method to better constrain halogen abundance in Earth's silicate reservoirs. Our method applies the log-log linear model of halogen and reference elements in MORB and OIB to estimate the halogen abundances in the respective source mantle (e.g., blue lines in Fig. 1 *B* and *C*). In this study, we consider the following four kinds of source mantle. The BSE refers to the chemical composition of mantle after core segregation and before the extraction of continental crust (CC); BSE is synonymous with the primitive mantle (PM). The depleted mantle (DM) denotes the residual mantle after the extraction of CC from BSE and can be further divided into the depleted MORB-source mantle (DMM) and the enriched OIB-source mantle (EM). DMM is more depleted in trace elements compared to EM.

By exploiting nonlinear correlations exhibited by MORB and OIB, our method can bypass the uncertainties of the bulk distribution coefficients of halogens during both mantle melting and magma crystallization (e.g., ref. 20), and compared to the constant ratio method, our approach results in notably higher halogen abundance in DMM and EM according to the MORB and OIB datasets (21) (https://search.earthchem.org/). In contrast to previous studies, this higher estimate suggests that halogen is not notably depleted in BSE compared to CI chondrites given their condensation temperatures, which indicates effective halogen preservation during planetary formation. Considering the history of mantle degassing (e.g., ref. 22) and the evolution of crustal recycling (e.g., ref. 23), our BSE estimate also suggests a halogen cycle of early degassing followed by a net regassing during the Earth history, which provides important implications for the evolution of ocean alkalinity and pH.

In what follows, we first present a brief description of our method based on a log-log linear model, then summarize the model results, and discuss the implications of our estimate of halogen abundance in BSE. The full description of our method and a detailed discussion on the problems of the constant ratio method are given in *Methods*.

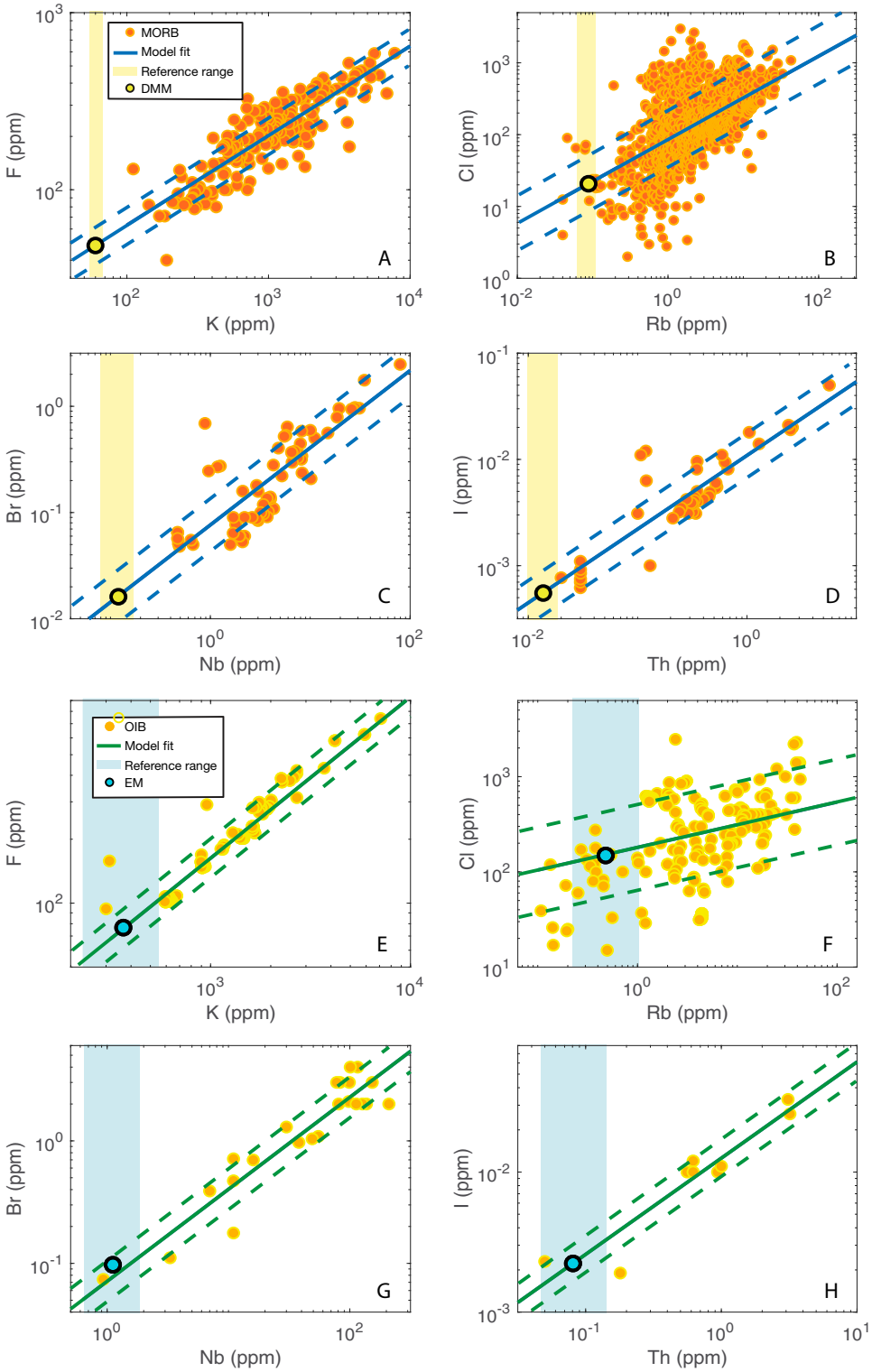

Fig. 2. Selected covariations between halogens and reference elements and their corresponding log-log linear models in MORB and OIB. (*A*) F versus K, (*B*) Cl versus Rb, (*C*) Br versus Nb, and (*D*) I versus Th in MORB. Orange dots are MORB data from PetDB (21). Blue solid and dashed lines are log-log linear models and their uncertainty ranges, respectively. Yellow bars and dots represent the concentrations of reference elements and halogens, respectively, in the DMM. *E–H* are the same with *A–D*, but for OIB data, shown as yellow dots, from PetDB (21). Green solid and dashed lines are log-log linear models and their uncertainty ranges, respectively. Blue bars and dots represent the concentrations of reference elements and halogens, respectively, in the EM.

Results

In addition to the use of a log-log linear model, our method is designed to obtain internally consistent halogen abundances in DMM, EM, DM, and BSE. For each halogen element, we first choose several reference elements, which have sufficiently high correlation coefficients with halogens in the log-log space (*SI Appendix*, Tables S1 and S2) and have good constraints on their abundances in CC, DMM, and BSE. A subset of the covariations between

Table 1. Halogen abundances in Earth's reservoirs, with the assumption that EM is the source mantle of OIB

	Mass (kg)	F (ppm)	Cl (ppm)	Br (ppb)	I (ppb)
Seawater (9)	1.40×10^{21}	1.3	1.93×10^{4}	6.6×10^{4}	60
Evaporites (28)	3.00×10^{19}	10	5.5×10^{5}	1.5×10^{5}	1.0×10^{3}
Crustal brines (26, 27)	6.00×10^{19}	20	1.0×10^{5}	6.0×10^{5}	1.5×10^{4}
Marine sediments (29)	5.00×10^{20}	1,000	4.0×10^{3}	4.0×10^{4}	3.0×10^{4}
CC (24)	2.09×10^{22}	553	244	880	700
EM (This study)	$1.21^{+0.8}_{-0.8} \times 10^{24}$	68^{+20}_{-16}	175^{+79}_{-55}	93^{+44}_{-30}	$2.2^{+0.81}_{-0.59}$
DMM (This study)	$2.81^{+0.8}_{-0.8} \times 10^{24}$	$48^{+5.3}_{-4.8}$	$26^{+10}_{-6.9}$	32^{+8}_{-6}	$0.5^{+0.10}_{-0.09}$
DM (This study)	4.02×10^{24}	$54^{+4.8}_{-4.4}$	67^{+26}_{-19}	49^{+10}_{-8}	$1.0^{+0.14}_{-0.12}$
BSE (This study)	4.04×10^{24}	$57^{+4.8}_{-4.4}$	81^{+24}_{-19}	91^{+19}_{-14}	$8.6^{+0.70}_{-0.61}$
Degassed from DM (This study)	—	5.24%	17.30%	46.59%	88.20%
BSE (9)	4.04×10^{24}	17 ± 6	26 ± 8	76 ± 25	7 ± 4
Degassed from DM (9)	—	51.08%	86.67%	88.14%	97.03%

halogens and reference elements in MORB and OIB and their corresponding log-log linear models are shown in Fig. 2, whereas the complete set of our results is provided in *SI Appendix*, Figs. S1–S5.

To make an internally consistent estimate of halogen abundances in Earth's silicate reservoirs, we then take the following five steps. First, according to the abundances of reference elements in CC (24) and BSE (12), we calculate their concentrations in DM using mass balance. Second, we calculate their concentrations in EM given their compositions in DM and DMM (25). Third, we obtain the halogen concentrations in DMM and EM using their log-log linear models with reference elements in MORB and OIB, respectively. Subsequently, the halogen compositions in DM can be calculated by summing their abundances in DMM and EM. Finally, we provide an estimate of BSE halogen budget by adding their abundances in surface reservoirs (9, 24, 26–29). Throughout these five steps, we use Monte Carlo sampling to incorporate the uncertainties of the relative proportion of DMM and EM (e.g., refs. 30 and 31), correlations between halogens and reference elements in MORB and OIB, and element concentrations in DMM (25), CC (24), and BSE (12). We have collected a total of 10,000 Monte Carlo sampling results, whose median and SD are reported in Table 1.

For the DMM composition, the models of Salters and Stracke (25) and Workman and Hart (32) have widely been used in the literature. In our analysis, we chose to use the former because the latter was found to result in negative EM abundances for some reference elements (e.g., Rb). The results in Table 1 are based on the assumption that DMM is the source mantle of MORB, whereas EM is the source mantle of OIB. We also tested the assumption that OIB was generated directly from BSE (which is synonymous with PM), and the corresponding results are provided in *SI Appendix*, Table S3, which displays higher halogen budgets in BSE. As seen in Table 1 and *SI Appendix*, Table S3, our method results in ∼2 to 9 times higher halogen concentrations in BSE compared to previous studies (e.g., refs. 9 and 11–13).

Given the halogen abundances in DM and BSE, we calculate their degassing fractions in the present-day mantle (Table 1 and *SI Appendix*, Table S3). Our BSE estimate suggests that less than one-half of each halogen have been degassed from the PM, with iodine as an exception (∼80%). A total amount of ∼87% stable halogens still reside in the mantle. Studies on halogen concentrations in serpentinites suggest that iodine and bromine are lost from serpentinites at shallower depths than chlorine and fluorine (e.g., ref. 33), which may be responsible for the higher degassing fractions of heavier halogens (Table 1 and *SI Appendix*, Table S3). Also, the calculated degassing fraction of iodine suggests that OIB cannot be generated directly from the PM (*SI Appendix*, Table S3). Whereas this high degassing fraction of iodine is subject to large uncertainties given the paucity of iodine data in the MORB and OIB datasets (*SI Appendix*, Tables S1 and S2), a better understanding of the mineral–melt–fluid partitioning of iodine is also warranted.

Discussion

As mentioned in the introductory section, previous studies of BSE halogen concentrations (e.g., refs. 9 and 11–13) exhibit a noteworthy depletion of Cl, Br, and I (green dots in Fig. 3), considering their condensation temperatures (14). This depletion has long been thought to require some peculiar halogen behaviors, including halogen sequestration into the core (15, 16), the lower condensation temperatures of halogens (17), and an impact-driven loss of halogens in the early Earth (13). However, our revised halogen abundances in BSE yield considerably higher CI-chondrite normalized values (red dots in Fig. 3), indicating that BSE is not unusually depleted in halogens. Thus, our results suggest sufficient halogen retention during planetesimal formation and giant impacts. Recently, Clay et al. (7) reexamined the abundances of chlorine, bromine, and iodine in various kinds of chondrites and reported much lower averaged concentrations of halogens. Normalizing our estimates to the chondrite values of Clay et al. (7) results in a halogen volatility trend slightly above the volatile lithophile elements with similar condensation temperatures (yellow dots in Fig. 3). The halogen concentrations of CI chondrites may not be as low as suggested by Clay et al. (7).

The previous estimates of the BSE budget yield a halogen degassing fraction of ∼80% from the present-day mantle (e.g., refs. 9, 18), which is considered to conflict with the mantle degassing fraction of ∼50% based on argon-40 (19). On the other hand, our results suggest much lower degassing fractions of halogens (∼5% for F to ∼47% for Br). It is important to understand that the degassing fractions of argon-40 and halogens do not have to be the same to begin with. First of all, unlike argon-40, halogens are not radiogenic; therefore, their degassing history can be more affected by early degassing events caused by giant impacts (e.g., ref. 34) and early intensive crustal generation and reworking (22). Argon-40, in contrast, did not exist in abundance in the early Earth because it is produced by the radioactive decay of potassium-40 with a half-life of over 1 billion years, so its present-day budget in the convecting mantle is much less sensitive to such early degassing. As fluorine and chlorine are most likely degassed in the form of HF and HCl, respectively, their degassing behavior is expected to be similar to that of water (35). Thus, based on water degassing expected during magma ocean solidification and subsequent mantle convection (e.g., refs. 36 and 37), halogens are likely to have been degassed efficiently during the Hadean. Moreover, halogens are more chemically active than argon and can be recycled into the mantle by chemically bonding to minerals. Thus, the lower degassing fraction of halogens suggested by our BSE budget is consistent with net halogen regassing

due to the recycling of both oceanic crust (e.g., ref. 23) and continental crust (e.g., ref. 22). A similar regassing history is reported for xenon (38) as well. The majority of halogens in the present-day mantle, originally brought as subducted materials, may exist along grain boundaries or in some trace minerals because nominally anhydrous minerals in mantle peridotites do not seem to contain a sufficient amount of halogens (39). As high concentrations of halogens are observed in both MORB and OIB, such mantle components enriched in halogens should be ubiquitous in the convecting mantle, though our study does not constrain their specifics.

To sum, our estimates suggest that the exchange of halogens between the surface and the interior is described by early degassing followed by net regassing through the rest of Earth history. Deep volatile cycle on Earth has long been investigated, as it can provide a framework for studying the long-term geochemical evolution of mantle, crust, and hydrosphere (e.g., refs. 8–10 and 40). Quantitative analyses have been conducted for quite a few elements, including water (e.g., refs. 37 and 40), carbon (e.g., refs. 41 and 42), sulfur (e.g., ref. 43), nitrogen (e.g., ref. 44), and noble gases (e.g., refs. 22 and 38). The proposed degassing history of halogens is a preliminary attempt in this thread of research, and future directions include the modeling of deep halogen cycle in conjunction with other geochemical and geophysical constraints and its application to relevant geological processes. For example, deciphering the evolution of ocean pH requires the understanding of both carbon and halogen cycles.

The geological history of ocean pH is critical in understanding the long-term habitability of Earth because it controls carbon partitioning within hydrosphere (45), biosynthetic pathways (46), and the stability of crustal and authigenic minerals (47). However, the early Earth environment is highly debated, with temperature estimates ranging from icy to hot (e.g., refs. 41 and 48) and ocean pH estimates fluctuating between strongly acidic to alkaline (41, 49, 50). To constrain the evolving seawater pH, one needs to solve the charge balance of the major seawater ions (e.g., ref. 51), including Na^+, Mg^{2+}, Cl^-, CO_3^{2-}, and SO_4^{2-}. Therefore, as one of the most important acids in the ocean, an accurate understanding of the outgassing history of chlorine is required to constrain the chemical properties of seawater. Previous efforts on constraining acid–base balance of the oceans mainly focus on exploring the effect of atmospheric pCO_2 (e.g., ref. 52), whereas the exchanges of chlorine among Earth reservoirs are parameterized simply by assuming a certain model for the thermal evolution of Earth (51). Modeling the history of halogen degassing based on our estimate of BSE budget will be an important step toward a comprehensive understanding of the geological history of ocean pH.

As explained in the introductory section, the constant ratio method is useful when estimating concentrations for element pairs with the same bulk distribution coefficients, but this requirement for bulk distribution coefficients is not easily satisfied. Because the constant ratio method has widely been used when building the compositional models of DMM (25, 32), CC (e.g., ref. 24), and BSE (e.g., refs. 11 and 12), it is important to revisit the validity of the constant ratio approach in those models. Our halogen budget, which depends on the models of major silicate reservoirs, must be seen as provisional until these models are thoroughly reexamined. The impact of this model dependence on our results is, however, likely to have been alleviated by incorporating various model uncertainties with Monte Carlo sampling. As many geochemical box models depend critically on global mass balance, an improved understanding of compositional models is essential for reconstructing global-scale geological processes.

Methods

Problems with the Constant Ratio Method. As mentioned in the introductory section, the ratio of halogen and reference element in MORB and OIB is used to calculate the halogen concentration in the respective source mantle, but this can lead to a severe underestimation. To demonstrate this point, we consider element concentrations in DMM and EM by assuming a two-stage model: the source mantle first generates primary melt, which then evolves to MORB or OIB through fractional crystallization. We begin with back-calculating element abundances in the primary melt from the composition of MORB or OIB. Here, we take the observed abundances of fluorine (F) and potassium (K) in MORB as an example, and their concentrations in the primary melt can be calculated as the following:

$$C_l(\mathrm{F}) = \frac{C_{\mathrm{MORB}}(\mathrm{F})}{f_C^{(D_C(\mathrm{F})-1)}}; \quad [1]$$

$$C_l(\mathrm{K}) = \frac{C_{\mathrm{MORB}}(\mathrm{K})}{f_C^{(D_C(\mathrm{K})-1)}}, \quad [2]$$

where C_l is the element concentration in the primary melt before fractional crystallization, C_{MORB} is the element concentration observed in MORB (black dot in Fig. 1*A*), and f_C and D_C are the melt fraction and bulk distribution coefficient during the fractional crystallization of primary melt. By taking the logarithm of Eqs. **1** and **2** and eliminating $\ln(f_C)$, the logarithmic concentrations of F and K in the primary melt are related as the following:

$$\ln\left(C_l(\mathrm{F})\right) = s\ln\left(C_l(\mathrm{K})\right) + \ln\left(\frac{C_{\mathrm{MORB}}(\mathrm{F})}{C_{\mathrm{MORB}}(\mathrm{K})^s}\right), \quad [3]$$

where the slope, s, is a function of the bulk distribution coefficients of F and K:

$$s = \frac{D_C(\mathrm{F}) - 1}{D_C(\mathrm{K}) - 1}. \quad [4]$$

By varying f_C and D_C, we calculate the possible concentrations of F and K in the primary melt. As can be seen from Eq. **4** and Fig. 1*A*, the slope of F and K in the primary melt is unity only when $D_C(\mathrm{F})$ and $D_C(\mathrm{K})$ are the same, which is what is assumed by the constant ratio method. In contrast, most of the observed log-covariations of halogen and reference elements in MORB and OIB exhibit a slope much less than unity (*SI Appendix*, Tables S1 and S2), which is equivalent to considerably higher halogen abundances in the primary melt.

We next consider the relation between the source mantle composition and the primary melt composition. Continuing with elements F and K, their concentrations in the source mantle may be calculated as:

$$C_{\mathrm{SM}}(\mathrm{F}) = \frac{C_l(\mathrm{F}) f_M}{1 - (1 - f_M)^{\frac{1}{D_M(\mathrm{F})}}}; \quad [5]$$

$$C_{\mathrm{SM}}(\mathrm{K}) = \frac{C_l(\mathrm{K}) f_M}{1 - (1 - f_M)^{\frac{1}{D_M(\mathrm{K})}}}, \quad [6]$$

where C_{SM} is the element concentration in the source mantle of MORB, C_l is the element concentration in the primary melt (black dots in Fig. 1*B*), and f_M and D_M are melt fraction and bulk distribution coefficient during fractional melting (53). By varying f_M and D_M, the concentrations of F and K in the MORB source mantle display a range of log-correlations (Fig. 1*B*), and we calculate the corresponding F concentrations in DMM (gray dots in Fig. 1*B*) using K abundance (gray bar in Fig. 1*B*).

The ratios of element concentrations in MORB and DMM equal to each other only when the bulk distribution coefficients of relevant elements are the same during both mantle melting and subsequent crystallization (Fig. 1*B*), which is required for the constant ratio method to be safely applied. However, the MORB and OIB data do not provide any pair of elements with a logarithmic slope of unity (*SI Appendix*, Tables S1 and S2), undermining the validity of the constant ratio method. Also, the covariation of element concentrations can change during mantle melting and crystallization, when their bulk distribution coefficients are different (Fig. 1 *A* and *B*). This suggests that even the observed log-linear relationship of element abundances in MORB or OIB may not simply be extrapolated to estimate halogen abundances in the respective source mantle. In summary, using the constant ratio method will cause severe underestimation of halogen abundances in DMM and EM.

A Method Based on a Log-Log Linear Model. Our method uses log-linear covariations between halogens and reference elements in MORB and OIB to estimate halogen abundances in their respective mantle. The bulk distribution coefficients of halogens can vary during both melting and crystallization (e.g., ref. 20), thus the simple extrapolation used in our method (dashed blue line in Fig. 1*B*) may be simplistic, but most of correlations considered here extend down to the level of concentration expected for a source mantle (Fig. 2 and *SI Appendix*, Figs. S1–S5). It is thus notable that, for any given pair of halogen and reference element with a logarithmic slope smaller than unity, our method results in considerably higher halogen abundances compared to the

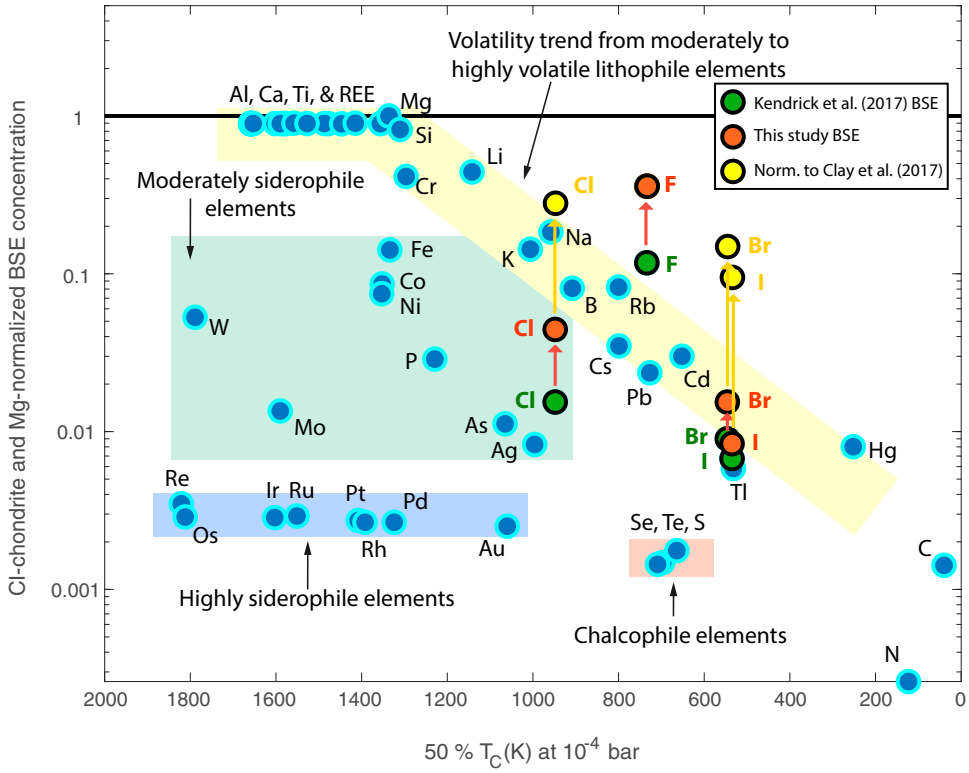

Fig. 3. CI-chondrite and Mg-normalized BSE abundance as a function of 50% condensation temperature (T_c). Blue dots are element concentrations in BSE (12) normalized to CI-chondrite and Mg. Yellow, green, blue, and pink bars represent the trend of moderately to highly volatile lithophile elements, moderately siderophile elements, highly siderophile elements, and chalcophile elements, respectively. Green dots are previous estimate of halogen concentration in BSE (9) normalized to CI-chondrite and Mg (11). Red dots are our estimates of halogen concentration in BSE normalized to CI-chondrite and Mg (11). Yellow dots are our estimates of halogen concentration in BSE normalized to the CI-chondrite composition of Clay et al. (7), and Mg. Values of 50% T_C are taken from Lodders (14).

constant ratio method (Fig. 1*C*). The slope of the fitted log-log linear model depends on the bulk distribution coefficients of both halogen and reference element (Eq. **4**), whereas the *y*-intercept reflects the average concentration of halogen in MORB or OIB (Eq. **3**). As both MORB and OIB are generally more evolved than their primary melts, the observed log-log linear relationships are dictated by fractional crystallization.

Based on the relationship of logarithmic slopes and the bulk distribution coefficients of relevant elements (Eq. **4**), the bulk distribution coefficients of halogens between mineral assemblage and basaltic melt can be estimated. As the reference elements used in our study are all highly incompatible (i.e., $D \ll 1$), the distribution coefficient for halogen may simply be estimated as $1 - s$, where s is the logarithmic slope. Estimated bulk distribution coefficients are ~0.55 for fluorine, ~0.5 for chlorine, ~0.35 for bromine, and ~0.3 for iodine. Heavier halogens are more incompatible, which is consistent with trends seen in experimental results for halogen partitioning. However, experimentally determined mineral-melt partition coefficients are lower often by more than one order of magnitude for nominally anhydrous minerals relevant to the solidification of basaltic melt (e.g., refs. 54 and 55). We note that the published partitioning experiments were conducted at pressures higher than those relevant to crystallization within the oceanic crust and that the pressure dependence of partitioning is indicated by some experimental data (54). Moreover, based on natural samples, Urann et al. (39) estimated the intermineral partitioning of fluorine and chlorine between mantle minerals, which differs significantly from what is suggested by the partitioning experiments. In our analysis, correlations involving chlorine are admittedly noisy likely because of seawater contamination as well as the assimilation of altered oceanic crust. However, correlations involving other halogens do not suffer from the same issue. Thus, the logarithmic correlations reported in this study may be considered as empirical constraints on the partitioning of these halogens, at least for the low-pressure fractionation of basaltic melt.

For each halogen element, we choose multiple reference elements to estimate the halogen abundance in BSE based on a log-log linear model. Reference elements are selected according to the following two criteria: 1) they have good correlation in the log-log space with halogen in both MORB and OIB (*SI Appendix*, Tables S1 and S2) and 2) they have well-constrained abundances in DMM, CC, and BSE. The concentrations of halogen and reference elements in MORB and OIB are taken from PetDB (21) using spreading center and off-axis spreading center as tectonic settings for MORB dataset, whereas oceanic island, seamount, oceanic plateau, and aseismic ridge were the settings for OIB dataset. The data are further selected by their MgO contents, to be within the range of 5 to 15%.

Taking F and K as an example again, we apply the following five steps, with log-log linear models and Monte Carlo sampling, to estimate F abundances in DMM, EM, DM, and BSE. First, by using the mass balance among DM, CC, and BSE, we calculate the concentration of K in DM as follows:

$$C_{DM}(K)M_{DM} = C_{BSE}(K)M_{BSE} - C_{CC}(K)M_{CC}, \quad [7]$$

where $C_{BSE}(K)$ and $C_{CC}(K)$ are the concentrations of K in BSE (12) and CC (24), respectively. Using Monte Carlo sampling, we take into account the uncertainties of element concentrations in BSE and CC. The masses of BSE (M_{BSE}) and CC (M_{CC}) are 4.0359×10^{24} kg and 2.09×10^{22} kg, respectively, whereas the mass of DM (M_{DM}) is the difference between M_{BSE} and M_{CC}.

Second, we calculate the concentration of K in EM [$C_{EM}(K)$] using the mass balance among DMM, EM, and DM as follows:

$$C_{EM}(K)M_{EM} = C_{DM}(K)M_{DM} - C_{DMM}(K)M_{DMM}, \quad [8]$$

where the concentration of K in DMM (C_{DMM}) is taken from Salters and Stracke (25). We incorporate the uncertainties of C_{DMM} and the relative proportion of M_{DMM} and M_{EM} using Monte Carlo sampling, where M_{DMM} is considered to be within the range of 70% ± 20% of M_{DM} (e.g., refs. 30 and 31).

Third, we calculate the concentrations of F in DMM and EM [$C_{DMM}(F)$ and $C_{EM}(F)$] based on a log-log linear model as follows:

$$C_{DMM}(F) = s_{MORB}C_{DMM}(K) + b_{MORB}, \quad [9]$$

$$C_{EM}(F) = s_{OIB}C_{EM}(K) + b_{OIB}, \quad [10]$$

where s and b are the log-slope and *y*-intercept of F and K covariation in MORB or OIB, respectively. The error envelopes of the log-log linear models are incorporated using Monte Carlo sampling. During this step, we use several reference elements for each halogen element to constrain their concentrations and take the medians as the halogen concentrations in DMM and EM.

Fourth, we estimate halogen abundance in the present-day DM [$C_{DM}(F)$] as follows:

$$C_{DM}(F)M_{DM} = C_{DMM}(F)M_{DMM} + C_{EM}(F)M_{EM}, \quad [11]$$

where M_{DMM} and M_{EM} are those sampled in the second step.

Last, by adding the abundances of halogen in Earth's surface reservoirs, we calculated the total halogen concentrations in BSE:

$$C_{DM}(F)M_{DM} + C_{SW}(F)M_{SW} + C_{EV}(F)M_{EV} + C_{CB}(F)M_{CB} + C_{MS}(F)M_{MS} + C_{CC}(F)M_{CC} = C_{BSE}(F)M_{BSE}, \quad [12]$$

where C_{SW}, C_{EV}, C_{CB}, C_{MS}, and C_{CC} are the concentrations of halogen in seawater (9), evaporites (28), crustal brines (26, 27), marine sediments (29), and CC (24), respectively, and M_{SW}, M_{EV}, M_{CB}, M_{MS}, and M_{CC} denote the masses of these reservoirs (Table 1). By construction, these five steps provide us an internally consistent estimate of halogen abundances in EM, DMM, DM, and BSE.

Data Availability. PetDB data have been deposited in Mendeley Data (21). All other study data are included in the article and/or *SI Appendix*.

ACKNOWLEDGMENTS. This article is supported by the NSF under Grant No. EAR-1753916 and the US National Aeronautics and Space Administration under Cooperative Agreement No. 80NSSC19M0069 issued through the Science Mission Directorate. We thank the editor and two anonymous reviewers for constructive comments.

1. M. A. Kendrick, "Halogens in seawater, marine sediments and the altered oceanic lithosphere" in *The Role of Halogens in Terrestrial and Extraterrestrial Geochemical Processes: Surface, Crust, and Mantle*, D. E. Harlov, L. Aranovich, Eds. (Springer, Cham, 2018), pp. 591–648.
2. D. R. Baker, H. Balcone-Boissard, Halogen diffusion in magmatic systems: Our current state of knowledge. *Chem. Geol.* **263**, 82–88 (2009).
3. P. Lecumberri-Sanchez, R. J. Bodnar, "Halogen geochemistry of ore deposits: Contributions towards understanding sources and processes" in *The Role of Halogens in Terrestrial and Extraterrestrial Geochemical Processes: Surface, Crust, and Mantle*, D. E. Harlov, L. Aranovich, Eds. (Springer, Cham, 2018), pp. 261–305.
4. D. Dolejš, Z. Zajacz, "Halogens in silicic magmas and their hydrothermal systems" in *The Role of Halogens in Terrestrial and Extraterrestrial Geochemical Processes: Surface, Crust, and Mantle*, D. E. Harlov, L. Aranovich, Eds. (Springer, Cham, 2018), pp. 431–543.
5. R. Fuge, "Soils and iodine deficiency" in *Essentials of Medical Geology*, O. Selinus *et al.*, Eds. (Elsevier Academic Press, Amsterdam, 2005), pp. 417–433.
6. G. M. El Zokm, M. M. Ismail, G. F. El-Said, Halogen content relative to the chemical and biochemical composition of fifteen marine macro and micro algae: Nutritional value, energy supply, antioxidant potency, and health risk assessment. *Environ. Sci. Pollut. Res. Int.* **28**, 14893–14908 (2021).
7. P. L. Clay *et al.*, Halogens in chondritic meteorites and terrestrial accretion. *Nature* **551**, 614–618 (2017).
8. R. D. Jarrard, Subduction fluxes of water, carbon dioxide, chlorine, and potassium. *Geochem. Geophys. Geosystems* **4**, 8905 (2003).
9. M. A. Kendrick *et al.*, Seawater cycled throughout Earth's mantle in partially serpentinized lithosphere. *Nat. Geosci.* **10**, 222–228 (2017).
10. H. Tang, D. Trail, E. A. Bell, T. M. Harrison, Zircon halogen geochemistry: Insights into Hadean-Archean fluids. *Geochem. Perspect. Lett.* **9**, 49–53 (2019).
11. W. F. McDonough, S. S. Sun, The composition of the Earth. *Chem. Geol.* **120**, 223–253 (1995).
12. T. Lyubetskaya, J. Korenaga, Chemical composition of Earth's primitive mantle and its variance: 1. Method and results. *J. Geophys. Res. Solid Earth* **112**, B03211 (2007).
13. Z. D. Sharp, D. S. Draper, The chlorine abundance of Earth: Implications for a habitable planet. *Earth Planet. Sci. Lett.* **369**, 71–77 (2013).
14. K. Lodders, Solar system abundances and condensation temperatures of the elements. *Astrophys. J.* **591**, 1220–1247 (2003).
15. W. F. McDonough, "Compositional model for the Earth's core" in *Treatise on Geochemistry*, R. W. Carlson, Ed. (Elsevier-Pergamon, Oxford, 2003), pp. 547–568.
16. R. M. G. Armytage, A. P. Jephcoat, M. A. Bouhifd, D. Porcelli, Metal-silicate partitioning of iodine at high pressures and temperatures: Implications for the Earth's core and ^{129}Xe budgets. *Earth Planet. Sci. Lett.* **373**, 140–149 (2013).
17. M. Y. Zolotov, M. Mironenko, "Hydrogen chloride as a source of acid fluids in parent bodies of chondrites" in *38th Lunar and Planetary Science Conference* (Lunar and Planetary Science XXXVIII 38, 2007), p. 2340.
18. R. Burgess, E. Layzelle, G. Turner, J. W. Harris, Constraints on the age and halogen composition of mantle fluids in Siberian coated diamonds. *Earth Planet. Sci. Lett.* **197**, 193–203 (2002).
19. C. J. Allègre, A. Hofmann, K. O'Nions, The argon constraints on mantle structure. *Geophys. Res. Lett.* **23**, 3555–3557 (1996).
20. J. D. Webster, D. R. Baker, A. Aiuppa, "Halogens in mafic and intermediate-silica content magmas" in *The Role of Halogens in Terrestrial and Extraterrestrial Geochemical Processes: Surface, Crust, and Mantle*, D. Harlow, L. Y. Aranovich, Eds. (Springer International Publishing, 2018), pp. 307–430.
21. M. Guo, J. Korenaga, MORB and OIB Halogen dataset from PetDB. Mendeley Data. https://doi.org/10.17632/yt4kts9sdp.1. Deposited 13 December 2021.
22. M. Guo, J. Korenaga, Argon constraints on the early growth of felsic continental crust. *Sci. Adv.* **6**, eaaz6234 (2020).
23. S. B. Shirey *et al.*, Archean emplacement of eclogite components into the lithospheric mantle during formation of the Kaapvaal Craton. *Geophys. Res. Lett.* **28**, 2509–2512 (2001).
24. R. L. Rudnick, S. Gao, "Composition of the continental crust" in *Treatise on Geochemistry*, H. D. Holland, K. K. Turekian, Eds. (Elsevier-Pergamon, 2003), **vol. 3**, pp. 1–64.
25. V. J. Salters, A. Stracke, Composition of the depleted mantle. *Geochem. Geophys. Geosystems* **5**, Q05004 (2004).
26. M. A. Kendrick, D. Phillips, M. Wallace, J. M. Miller, Halogens and noble gases in sedimentary formation waters and Zn-Pb deposits: A case study from the Lennard Shelf, Australia. *Appl. Geochem.* **26**, 2089–2100 (2011).
27. R. H. Worden, Controls on halogen concentrations in sedimentary formation waters. *Mineral. Mag.* **60**, 259–274 (1996).
28. W. W. Hay *et al.*, Evaporites and the salinity of the ocean during the Phanerozoic: Implications for climate, ocean circulation and life. *Palaeogeogr. Palaeoclimatol. Palaeoecol.* **240**, 3–46 (2006).
29. Y. Muramatsu *et al.*, Halogen concentrations in pore waters and sediments of the Nankai Trough, Japan: Implications for the origin of gas hydrates. *Appl. Geochem.* **22**, 534–556 (2007).
30. S. B. Jacobsen, G. J. Wasserburg, The mean age of mantle and crustal reservoirs. *J. Geophys. Res.* **84**, 7411–7427 (1979).
31. A. W. Hofmann, Mantle geochemistry: The message from oceanic volcanism. *Nature* **385**, 219–229 (1997).
32. R. K. Workman, S. R. Hart, Major and trace element composition of the depleted MORB mantle (DMM). *Earth Planet. Sci. Lett.* **231**, 53–72 (2005).
33. M. A. Kendrick *et al.*, Subduction zone fluxes of halogens and noble gases in seafloor and forearc serpentinites. *Earth Planet. Sci. Lett.* **365**, 86–96 (2013).
34. R. O. Pepin, D. Porcelli, Xenon isotope systematics, giant impacts, and mantle degassing on the early Earth. *Earth Planet. Sci. Lett.* **250**, 470–485 (2006).
35. P. J. Wallace, A. F. Anderson, "Volatiles in magmas" in *Encyclopedia of Volcanoes*, H. Sigurdsson, Ed. (Wiley, New York, 2000), pp. 149–163.
36. J. Korenaga, Hadean geodynamics and the nature of early continental crust. *Precambrian Res.* **359**, 106178 (2021).
37. J. Korenaga, N. J. Planavsky, D. A. D. Evans, Global water cycle and the coevolution of the Earth's interior and surface environment. *Philos. Trans.- Royal Soc., Math. Phys. Eng. Sci.* **375**, 20150393 (2017).
38. R. Parai, S. Mukhopadhyay, Xenon isotopic constraints on the history of volatile recycling into the mantle. *Nature* **560**, 223–227 (2018).
39. B. M. Urann *et al.*, Fluorine and chlorine in mantle minerals and the halogen budget of the Earth's mantle. *Contrib. Mineral. Petrol.* **172**, 51 (2017).
40. E. Ito, D. M. Harris, A. T. Anderson Jr., Alteration of oceanic crust and geologic cycling of chlorine and water. *Geochim. Cosmochim. Acta* **47**, 1613–1624 (1983).
41. N. H. Sleep, K. Zahnle, Carbon dioxide cycling and implications for climate on ancient Earth. *J. Geophys. Res. Planets* **106**, 1373–1399 (2001).
42. M. M. Hirschmann, Comparative deep Earth volatile cycles: The case for C recycling from exosphere/mantle fractionation of major (H_2O, C, N) volatiles and from H_2O/Ce, CO_2/Ba, and CO_2/Nb exosphere ratios. *Earth Planet. Sci. Lett.* **502**, 262–273 (2018).
43. T. Kagoshima *et al.*, Sulphur geodynamic cycle. *Sci. Rep.* **5**, 8330 (2015).
44. A. Mallik, Y. Li, M. Wiedenbeck, Nitrogen evolution within the Earth's atmosphere-mantle system assessed by recycling in subduction zones. *Earth Planet. Sci. Lett.* **482**, 556–565 (2018).
45. R. A. Feely, S. C. Doney, S. R. Cooley, Ocean acidification: Present conditions and future changes in a high-CO_2 world. *Oceanography (Wash. D.C.)* **22**, 36–47 (2009).
46. W. Runguphan, X. Qu, S. E. O'Connor, Integrating carbon-halogen bond formation into medicinal plant metabolism. *Nature* **468**, 461–464 (2010).
47. J. L. Palandri, Y. K. Kharaka, "A compilation of rate parameters of water-mineral interaction kinetics for application to geochemical modeling" (Open-File Rep. 2004-1068, US Geological Survey, 2004).
48. F. Robert, M. Chaussidon, A palaeotemperature curve for the Precambrian oceans based on silicon isotopes in cherts. *Nature* **443**, 969–972 (2006).
49. J. P. Grotzinger, J. F. Kasting, New constraints on Precambrian ocean composition. *J. Geol.* **101**, 235–243 (1993).
50. S. Kempe, E. T. Degens, An early soda ocean? *Chem. Geol.* **53**, 95–108 (1985).
51. I. Halevy, A. Bachan, The geologic history of seawater pH. *Science* **355**, 1069–1071 (2017).
52. J. Krissansen-Totton, G. N. Arney, D. C. Catling, Constraining the climate and ocean pH of the early Earth with a geological carbon cycle model. *Proc. Natl. Acad. Sci. U.S.A.* **115**, 4105–4110 (2018).
53. C. H. Langumuir, E. M. Klein, T. Plank, "Petrological systematics of mid-ocean ridge basalts: Constraints on melt generation beneath ocean ridges" in *Mantle Flow and Melt Generation at Mid-Ocean Ridges*, J. P. Morgan, D. K. Blackman, J. M. Sinton, Eds. (*Geophysical Monograph Series*, American Geophysical Union, 1992), pp. 183–280.
54. C. Dalou, K. T. Koga, N. Shimizu, J. Boulon, J. L. Devidal, Experimental determination of F and Cl partitioning between lherzolite and basaltic melt. *Contrib. Mineral. Petrol.* **163**, 591–609 (2012).
55. C. Dalou, K. T. Koga, M. Le Voyer, N. Shimizu, Contrasting partition behavior of F and Cl during hydrous mantle melting: Implications for Cl/F signature in arc magmas. *Prog. Earth Planet. Sci.* **1**, 1–17 (2014).